



**HAL**  
open science

## Sub-ppb mercury detection in real environmental samples with an improved Rhodamine-based detection system

Sukhdev Singh, Bruno Coulomb, Jean-Luc Boudenne, Damien Bonne, Frédéric Dumur, Bertrand Simon, F. Robert-Peillard

### ► To cite this version:

Sukhdev Singh, Bruno Coulomb, Jean-Luc Boudenne, Damien Bonne, Frédéric Dumur, et al.. Sub-ppb mercury detection in real environmental samples with an improved Rhodamine-based detection system. *Talanta*, 2021, pp.121909. 10.1016/j.talanta.2020.121909 . hal-03026250

**HAL Id: hal-03026250**

**<https://amu.hal.science/hal-03026250v1>**

Submitted on 26 Nov 2020

**HAL** is a multi-disciplinary open access archive for the deposit and dissemination of scientific research documents, whether they are published or not. The documents may come from teaching and research institutions in France or abroad, or from public or private research centers.

L'archive ouverte pluridisciplinaire **HAL**, est destinée au dépôt et à la diffusion de documents scientifiques de niveau recherche, publiés ou non, émanant des établissements d'enseignement et de recherche français ou étrangers, des laboratoires publics ou privés.

# Sub-ppb mercury detection in real environmental samples with an improved Rhodamine-based detection system

Sukhdev Singh<sup>2</sup>, Bruno Coulomb<sup>1</sup>, Jean-Luc Boudenne<sup>1</sup>, Damien Bonne<sup>2</sup>, Frédéric Dumur<sup>3</sup>, Bertrand Simon<sup>4</sup>, Fabien Robert-Peillard<sup>1\*</sup>

<sup>1</sup>Aix Marseille Univ, CNRS, LCE, Marseille, France

<sup>2</sup>Aix Marseille Université, CNRS, Centrale Marseille, iSm2, Marseille, France

<sup>3</sup> Aix Marseille Univ, CNRS, ICR, UMR 7273, F-13397 Marseille France

<sup>4</sup> Institut d'Optique & CNRS, Laboratoire Photonique Numérique et Nanoscience, UMR 5298, Talence, France

\*Corresponding author: fabien.robert-peillard@univ-amu.fr

## Abstract

A new procedure is described for the determination of Hg<sup>2+</sup> ions in water samples. A Rhodamine based fluorescent sensor was synthesized and the experimental conditions were specifically optimized for application to environmental samples, which requires low detection limits and high selectivity in competitive experiments with realistic concentrations of other metal ions. Incorporation of a Rhodamine-6G fluorophore to a previously described sensor and optimization of the buffer system (detection with acetic acid at pH 5.25) enabled significant enhancement of the sensitivity (detection limit = 0.27 µg.L<sup>-1</sup>) and selectivity. The optimized procedure using high-throughput microplates has been applied to tap and river waters with good results.

**Keywords:** Fluorescent sensor; Mercury ion; Rhodamine derivative; Water analysis.

## 1. Introduction

Mercury is one of the most toxic metals found in the environment, with well-known deleterious effects on kidneys, liver and the central nervous system which leads to various cognitive and

28 motor disorders [1,2]. Among mercury species, the  $\text{Hg}^{2+}$  ion has been extensively studied  
29 because it can be biomethylated into methyl mercury in the environment [3]. Conventional  
30 methods for analysis of mercury in laboratories include cold vapor atomic absorption  
31 spectroscopy and inductively coupled plasma mass spectrometry, which are either expensive or  
32 complex analytical techniques. Methods based on fluorescent sensors have gained considerable  
33 attention in the past years, due to the simplicity of the operations combined to high selectivity  
34 and sensitivity of the designed sensors.

35 Fluorescent sensors based on organic dyes are particularly suited for the analysis of  $\text{Hg}^{2+}$  ion  
36 and other cations [4-6]. This type of sensor includes an ion recognition unit (ionophore) which  
37 triggers modification of the fluorescence features of an organic fluorophore. Among these  
38 fluorophores, the rhodamine framework has appeared as the ideal choice, due to the high  
39 fluorescence quantum yields obtained by the spiro-lactam cycle opening and the ease of  
40 structural modification for the ionophore part. Consequently, several Rhodamine-based  
41 molecular sensors for  $\text{Hg}^{2+}$  have been described in the literature [7].

42 However, most of these sensors have not convincingly demonstrated their capacities to be  
43 applied to the analysis of real environmental waters (tap water, natural waters). To fulfill  
44 requirements for these types of analysis, the sensor has to: i) detect mercury in aqueous media;  
45 ii) reach high sensitivity with quantification limits below the  $\mu\text{g.L}^{-1}$  range (the parametric value  
46 for the quality of water intended for human consumption in Europe is  $1 \mu\text{g.L}^{-1}$  and the maximal  
47 allowable concentration in inland waters has been established to  $0.05 \mu\text{g.L}^{-1}$  by European  
48 Union); iii) prove the selectivity for  $\text{Hg}^{2+}$  in the presence of very large excess of some other  
49 naturally occurring ions (especially  $\text{Ca}^{2+}$  or  $\text{Cu}^{2+}$ ). Regarding application to aqueous sample,  
50 rhodamine-based sensors displaying interesting analytical features only in organic or mixed  
51 organic-aqueous media will not be efficient [8,9]. Likewise, many sensors have detection limits  
52 which are either not indicated or in the  $10^{-8}$ - $10^{-6}$  M range ( $2$ - $200 \mu\text{g.L}^{-1}$ ) [10-12], which is not

53 enough sensitive for real samples like tap water or natural waters. Selectivity for  $\text{Hg}^{2+}$  is almost  
54 always demonstrated by competitive experiments with 1-10 equivalents of other metal ions  
55 compared to mercury [10, 12-16], which is not representative of real environmental samples.  
56 Application of Rhodamine fluorescent sensors is thus generally limited to the fluorescence  
57 imaging of  $\text{Hg}^{2+}$  in cells. Only one application to real water samples has been documented by  
58 Pan et al. with the determination of  $\text{Hg}^{2+}$  in industrial wastewaters in the  $\mu\text{M}$  range (150-250  
59  $\mu\text{g.L}^{-1}$ ) [17]. Description of a rhodamine sensor designed for tap or natural water analysis is  
60 thus highly needed.

61 Among rhodamine sensors,  $\text{NS}_2$  ionophore described by Huang et al. [15] seemed particularly  
62 suited for aqueous application with high selectivity for  $\text{Hg}^{2+}$ . In the present study we  
63 synthesized the rhodamine B sensor (sensor S2, Fig. 1) described by Huang et al. [15].  
64 However, the first experiments using their experimental conditions led us to conclude that the  
65 sensitivity seemed too low for application to environmental water samples. We thus decided to  
66 modify that sensor by incorporation of a rhodamine-6G fluorophore group (sensor S1) and to  
67 investigate analytical parameters in order to reach low  $\mu\text{g.L}^{-1}$  detection limit for application to  
68 real water samples. Experiments were performed in microplates to take advantage of the high-  
69 throughput screening properties of this type of analytical tool, ideal for optimization purposes.  
70 Results of these optimizations are reported in this work.

71

## 72 **2. Material and methods**

73

### 74 2.1. Chemicals and reagents

75 Rhodamine-6G (Dye content: 95%), HEPES (4-(2-Hydroxyethyl)piperazine-1-ethanesulfonic  
76 acid), MOPS (3-(N-Morpholino)propanesulfonic acid) and acetic acid were purchased from

77 Sigma-Aldrich (France). Ultrapure water purified with a Milli-Q system (Millipore, USA,  
78 resistivity >18 MΩ cm) was used for the preparations of the whole solutions.

79 A 1 mg.L<sup>-1</sup> Hg<sup>2+</sup> stock solution was prepared daily in a glass vial [18] by dilution of a 1 g.L<sup>-1</sup>  
80 standard solution (AAS grade, Sigma Aldrich) with ultrapure water and a few drops of NaOH  
81 0.1 M solution to set pH of the stock solution between 3.5-4. The same protocol was applied  
82 for the other heavy metal stock solutions used for the selectivity study.

83 5 mM stock solutions of sensors were prepared in DMSO and stored at +4° C (stable for at least  
84 2 months). The stock solution was then diluted in ultrapure water to give a 5 μM working  
85 solution (1 % DMSO), which was stable for at least 2 weeks in the fridge.

86 The tap water sample was collected in the laboratory (Marseille, France). River water samples  
87 were collected from the Huveaune (River 1: Roquevaire, France; River 2: Aubagne, France)  
88 and the Arc (River 3: Ventabren, France), filtered on 0.45 μm PES filters and stored at +4° C  
89 until analysis. pH of the spiked samples was set between 5.2 and 5.3 with diluted HNO<sub>3</sub> to  
90 avoid pH variation after addition of acetic acid buffer.

91

## 92 2.2.Synthesis of sensor **S1** and **S2**

93 The sensors **S1** was synthesized by a simple modified procedure starting from rhodamine-6G  
94 base (**1**) (Scheme 1, see supporting information for detailed procedure). The rhodamine-6G  
95 base **1** was reacted with ionophore **NS2** in the presence of 4-toluenesulfonyl chloride (TsCl)  
96 and 4-dimethylaminopyridine (DMAP) in dry dichloromethane at room temperature for 4 h and  
97 sensor **S1** was obtained in 47% yield as a light pink/beige color solid. <sup>1</sup>H NMR (400 MHz,  
98 CDCl<sub>3</sub>) δ 8.05-8.00 (m, 1H), 7.62-7.55 (m, 3H), 7.27-7.22 (m, 1H), 7.14 (td, 1H, *J* = 7.6 Hz,  
99 1.4 Hz), 6.84 (td, *J* = 7.7 Hz, 1.7 Hz), 6.34 (d, 2H, *J* = 5.4 Hz), 6.21 (s, 1H), 6.10 (s, 1H), 5.94

100 (dd, 1H,  $J = 8.0$  Hz, 1.4 Hz), 3.53 and 3.45 (2 x s, 2H), 3.34 (d, 1H,  $J = 15.8$  Hz), 3.23-3.03 (m,  
101 4H), 2.62 (d, 1H,  $J = 15.7$  Hz), 2.48-2.31 (m, 10H), 2.29-2.19 (m, 2H), 1.96 and 1.93 (2 x s,  
102 6H), 1.33-1.22 (m, 6H), 1.15 (t, 6H,  $J = 7.4$  Hz).  $^{13}\text{C}$  NMR (100 MHz,  $\text{CDCl}_3$ )  $\delta$  166.09, 153.49,  
103 152.93, 151.54, 147.81, 139.80, 133.86, 132.88, 132.80, 129.75, 128.80, 128.70, 128.62,  
104 128.18, 128.12, 126.48, 124.73, 123.61, 120.96, 118.12, 117.19, 108.45, 107.22, 96.88, 96.67,  
105 68.54, 54.52, 54.43, 38.61, 38.49, 30.11, 27.13, 26.22, 17.19, 17.02, 15.01, 14.86. HRMS (ED):  
106 Calculated for  $\text{C}_{41}\text{H}_{51}\text{N}_4\text{O}_2\text{S}_2$   $[\text{M}+\text{H}]^+$  695.3448; found: 695.3445.

107 Sensor **S2** was also synthesized using similar procedure as adopted for sensor **S1** starting with  
108 rhodamine-base B (**2**) and ionophore **NS2**. With this method, sensor **S2** was obtained as a beige  
109 color solid with improved 65% yield as compared to previously reported yield of 26% [15] (see  
110 supplementary data for detailed procedure and NMR data).

111

### 112 2.3. Instrumentation

113 Fluorescence spectra of sensor **S1** and sensor **S2** were recorded on a SAFAS Xenius  
114 spectrofluorometer (Monaco) equipped with a Xenon lamp and controlled by SP2000 V7  
115 software (SAFAS). Microplate fluorescence measurements were carried out on a microplate  
116 reader (Infinite M200, Tecan France SAS, Lyon, France) equipped with an excitation and  
117 emission double monochromator (bandwidths of 9 nm and 20 nm for excitation and emission  
118 monochromator, respectively) and controlled by i-control™ software (Tecan). Fluorescence  
119 detection was performed from above the microplate wells (top configuration), at  $\lambda_{\text{ex}} = 540$  nm  
120 and  $\lambda_{\text{em}} = 575$  nm. Operating temperature was set to 25 °C. Other parameters were as follows:  
121 gain: 180; number of flashes: 50; integration time: 20  $\mu\text{s}$ . Fluorescence intensities were  
122 expressed in arbitrary units (a.u.). Polypropylene black 96 well U-bottom microplates (Nunc),  
123 with a maximum capacity of 500  $\mu\text{L}$  for each well were used.

## 124 2.4. General microplate procedure

125 300  $\mu\text{L}$  of sample or  $\text{Hg}^{2+}$  standard solution were dispensed into the wells of the microplate,  
126 followed by 50  $\mu\text{L}$  of the buffer solution and 30  $\mu\text{L}$  of the 5  $\mu\text{M}$  working solution of sensor **S1**.  
127 The plate was shaken for 3 min in the microplate reader, and fluorescence was subsequently  
128 measured at  $\lambda_{\text{ex}} = 540 \text{ nm}$  and  $\lambda_{\text{em}} = 575 \text{ nm}$ . All experiments were performed in duplicate.

129

## 130 3. Results and discussion.

### 131 3.1. Optimization of experimental conditions

#### 132 3.1.1. Fluorescence response of **S1** and **S2** at pH 7

133 The publication from Huang et al. [15] studying **S2** used HEPES buffer at pH 7 (with 15%  
134 MeCN). Our first experiments with **S1** and **S2** displayed a negative influence of MeCN on the  
135 fluorescent response, so we decided to compare the response of the sensors only in pure aqueous  
136 solution. Our analytical protocol used a large volume of sample and addition of a small volume  
137 of buffer and sensor, to optimize the analytical performances of the protocol. Standard solutions  
138 of  $1 \text{ mg.L}^{-1} \text{ Hg}^{2+}$  were neutralized at pH around 4 (starting from stock solution in 5%  $\text{HNO}_3$ ) in  
139 order to avoid variation of pH between blank and standard solutions. Fluorescence emission  
140 spectra recorded on a traditional spectrofluorometer are displayed on Figure 2. As expected,  
141 emission wavelength (565 nm) for **S1** with Rhodamine-6G base is lower than **S2** (595 nm) with  
142 Rhodamine B base [10]. **S1** also already showed superior performances at low concentrations,  
143 with a fluorescence response at  $10 \text{ }\mu\text{g.L}^{-1}$  much better than **S2** (see inset of Fig. 2). We thus  
144 decided to focus on the new sensor with Rhodamine-6G for the optimization of the experimental  
145 conditions.

#### 146 3.1.2. Influence of the pH buffer

147 Most publications study the fluorescence response of the sensors at high concentrations of the  
148 metal cation targeted ( $1-10 \mu\text{M} = 200-2000 \mu\text{g.L}^{-1}$ ). Our aim was to develop a simple microplate  
149 protocol that could be used at low mercury concentrations more consistent with environmental  
150 conditions (linear range up to  $10 \mu\text{g.L}^{-1}$ , detection limit below  $1 \mu\text{g.L}^{-1}$ ), so we first studied the  
151 influence of the pH on  $10 \mu\text{g.L}^{-1}$  and  $2 \mu\text{g.L}^{-1}$  standard solutions. High-throughput microplates  
152 and a microplate reader were used for all the optimization tests. Results for various pH are  
153 presented on Figure 3 (MOPS was used at pH 7 with similar results as HEPES, with better  
154 buffer capacity for MOPS than HEPES at pH 7). Interestingly, evolution of the fluorescence  
155 response of the sensor is completely different at pH 5.25 compared to pH 7. While ratio between  
156 fluorescence response of a  $10 \mu\text{g.L}^{-1}$  and a blank solution is much better at pH 7, results are  
157 completely opposite for the  $2 \mu\text{g.L}^{-1}$  standard solution. In fact, only slightly acidic conditions  
158 (pH 5-5.5) can enable actual detection of standard solution of  $\text{Hg}^{2+}$  below  $2 \mu\text{g.L}^{-1}$  with **S1**.  
159 Buffers with pH below 5 displayed lower response with both standard solutions.

### 160 3.1.3. Influence of the sensor concentration

161 While better results with low concentration of sensor could be anticipated to improve sensitivity  
162 and detection limit [10], our experiments with **S1** did not display a sharp effect when sensor  
163 concentration was lowered (Fig. 4). Results were similar in the range  $0.5-5 \mu\text{M}$  but choosing a  
164 too low sensor concentration to optimize detection limit could be detrimental for selectivity in  
165 presence of other metal cations and both analytical aspects have to be taken into account when  
166 one optimize a protocol for application to real environmental samples. We thus decided to keep  
167  $5 \mu\text{M}$  as the optimal concentration value for the rest of the study.

### 168 3.1.4. Characterization of the complex between **S1** and $\text{Hg}^{2+}$

169 Regarding stoichiometry of the complex between **S1** and  $\text{Hg}^{2+}$ , the Job's Plot depicted in Figure  
170 S1 (for sensor **S1** at pH 5.25) proved the same 1:1 stoichiometry as sensor **S2** at pH 7 [15]. This



171 was also confirmed by ES(+)-HRMS of a mixture of **S1** and  $\text{Hg}^{2+}$  (Fig. S9, supplementary data),  
172 with a peak at 931.3174 assigned to the single-charged complex  $[\text{S1} + \text{Hg}^{2+} + \text{Cl}^-]^+$ . To further  
173 confirm the coordination of Sensor **S1** with  $\text{Hg}^{2+}$ ,  $^1\text{H-NMR}$  experiments were done. As shown  
174 in Figure S10 (supplementary data), the triplet peaks centered at  $\delta 1.20$  corresponding to methyl  
175 groups (1 and 1'), shifted downfield to  $\delta 1.41$  ( $\Delta\delta = 0.21$  ppm) upon addition of 1 equiv of  $\text{Hg}^{2+}$   
176 to the sensor **S1**. This shift was attributed to the coordination of sulphur "S" with  $\text{Hg}^{2+}$ .  
177 Moreover, the quartets and triplets associated with protons 2, 2', 3 and 3' also shifted to the  
178 downfield region of the spectra. The triplets due to the methylene groups attached nitrogen of  
179 ionophore part (4 and 4') also shown the shifts towards downfield region of the spectra which  
180 indicated the involvement of "N" in coordination with  $\text{Hg}^{2+}$ . The aromatic protons of  
181 rhodamine, specially  $\text{H}_6$ ,  $\text{H}_6'$ ,  $\text{H}_7$  and  $\text{H}_7'$  also shown the clear changes in their chemical shifts  
182 due to the shifting of the aromatic bonds (delocalization) that trigger opening of spirolactone  
183 upon complexation with  $\text{Hg}^{2+}$ . Based on combined results of NMR and HRMS analysis, we  
184 could propose the mode of coordination of sensor **S1** with  $\text{Hg}^{2+}$  as described in scheme S5  
185 (supplementary data) where both sulphur "S" and "N" of ionophore part, and "O" of carbonyl  
186 are involved in the interaction with  $\text{Hg}^{2+}$ .

187

## 188 3.2. Analytical performances of sensor **S1**

### 189 3.2.1. Comparison of the detection limit of **S1** and **S2**

190 Detection limits for **S1** and **S2** (calculated as  $3\sigma_b/s$ ;  $\sigma_b$  is the standard deviation of the blank  
191 signals with  $n=10$ , and  $s$  the slope of the calibration curve) were compared for various  
192 experimental conditions (Table 1). The first tests were carried out following the conditions  
193 described by Huang et al. for **S2** (with 15% acetonitrile). In our experiments, acetonitrile was  
194 not necessary for solubility purposes using the sensor concentration described (25  $\mu\text{L}$  of a 5  $\mu\text{M}$

195 sensor solution, corresponding to 0.33  $\mu\text{M}$  in the mixture with sample and buffer; Solutions of  
 196 **S1** at 5  $\mu\text{M}$  are stable in the fridge at least for 2 weeks after dilution of a 5 mM stock solution  
 197 in DMSO). At pH 7.1 and 5.25, sensor **S1** could detect mercury at concentrations 3.5 times  
 198 lower than **S2**, proving that rhodamine-6G base is better than rhodamine B for this type of  
 199 sensor (Table 1). To the best of our knowledge, this study is the first report which compares the  
 200 influence of the rhodamine fluorophore (with the same ionophore) on the sensitivity of a sensor.  
 201 An excellent detection limit of 0.3  $\mu\text{g.L}^{-1}$  (1.5 nM) could be obtained with acetic acid buffer,  
 202 proving high sensitivity of the new sensor with the optimized experimental parameters. Overall,  
 203 detection limits using this type of rhodamine sensor have been improved 175 times compared  
 204 to conditions described before using S2.

Experimental conditions	S1	S2
MeCN/HEPES 20 mM pH 7 (15/85) <sup>a</sup>	19 $\mu\text{g.L}^{-1}$	53 $\mu\text{g.L}^{-1}$
MOPS 50 mM pH 7.1 <sup>b</sup>	2.0 $\mu\text{g.L}^{-1}$	7.1 $\mu\text{g.L}^{-1}$
Acetic acid 50 mM pH 5.25 <sup>b</sup>	0.27 $\mu\text{g.L}^{-1}$	1.1 $\mu\text{g.L}^{-1}$

205 a. In the final mixture; b. Buffer added to the sample (50  $\mu\text{L}$  buffer for 300  $\mu\text{L}$  sample).

206 Table 1. Detection limits obtained with **S1** and **S2** using different conditions with the microplate  
 207 protocol. Detection wavelengths for S1:  $\lambda_{\text{exc}} = 535 \text{ nm}$ ;  $\lambda_{\text{em}} = 570 \text{ nm}$ ; for S2:  $\lambda_{\text{exc}} = 540 \text{ nm}$ ;  
 208  $\lambda_{\text{em}} = 595 \text{ nm}$ .

### 209 3.2.2. Analytical features for sensor **S1**

210 The analytical procedure with sensor **S1** was evaluated using the optimized experimental  
 211 conditions (Table 2). Very good linear regression coefficient was obtained in the range 0.9-20  
 212  $\mu\text{g.L}^{-1}$  (Fig S2), with excellent RSD value proving repeatability of our measurements. The limit  
 213 of quantification is below 1  $\mu\text{g.L}^{-1}$ , which is the parametric value for the quality of water

214 intended for human consumption in Europe [19]. The protocol can thus be implemented for this  
215 kind of samples regarding the European legislation.

<b>Limit of detection (<math>\mu\text{g.L}^{-1}</math>)</b>	0.27
<b>Limit of quantification (<math>\mu\text{g.L}^{-1}</math>)</b>	0.92
<b>Linear working range (<math>\mu\text{g.L}^{-1}</math>)</b>	0.9-20
<b>R<sup>2</sup></b>	0.997
<b>RSD (%)<sup>a</sup></b>	2.9

216 a. Calculated on a  $5 \mu\text{g.L}^{-1}$  standard, n= 6 replicates

217 Table 2. Analytical features of the microplate protocol with **S1**. Buffer: Acetic acid 50 mM pH  
218 5.25.

### 219 3.2.3. Selectivity study

220 Selectivity of a sensor for a metal ion is crucial for application to real samples. This is  
221 particularly important for mercury ion in environmental samples, with mercury concentration  
222 in the nM range, while other metal ions could be present up to a few tens of  $\mu\text{M}$  ( $\text{Cu}^{2+}$ ,  $\text{Zn}^{2+}$ ) or  
223 in the mM range ( $\text{Ca}^{2+}$ ,  $\text{Mg}^{2+}$ ). Most publications describe their selectivity study with  $\mu\text{M}$   
224 concentration of  $\text{Hg}^{2+}$  and 10 equivalents of other metal ion, which are experimental hypothesis  
225 clearly not suitable for environmental samples. For this study, we chose  $\text{Hg}^{2+}$  at  $5 \mu\text{g.L}^{-1}$  (25  
226 nM) in order to obtain a significant response with good repeatability. Concentrations of other  
227 metal ions were chosen based on parametric values defined by the European legislation on water  
228 intended for human consumption ( $\text{Cu}^{2+}$ ,  $\text{Pb}^{2+}$ ,  $\text{Cd}^{2+}$ ). For metal ions not listed in this legislation,  
229 we chose high concentrations that should not be exceeded in a surface water ( $\text{Ca}^{2+}$ ,  $\text{Mg}^{2+}$ ,  $\text{Zn}^{2+}$ ).  
230 Response was studied first with each metal ion separately and then under competitive  
231 conditions with mercury ion at  $5 \mu\text{g.L}^{-1}$  (Fig. 5). We also compared our optimized experimental

232 conditions (acetic acid buffer pH 5.25, Fig. 5A) with usual conditions used for this type of  
233 sensor (buffer at pH 7, Fig. 5B). The tolerance limit was  $\pm 5\%$  change between the fluorescence  
234 of  $\text{Hg}^{2+}$  alone and the fluorescence in presence of interfering ions at the maximal concentration  
235 chosen. Results display excellent selectivity of sensor **S1**, even in competitive experiments with  
236 other metal ions in real environmental concentrations (the tolerance limit was not exceeded for  
237 all metal ions studied). Interestingly for our study, the same experiment at neutral pH  
238 (conditions described by previous group studying sensor **S2**) gives strong interference of copper  
239 ions, completely inhibiting response of sensor **S1** with mercury ions. The same results were  
240 found with HEPES buffer. pH is thus an important parameter in our procedure to avoid  
241 interference from copper ions. Study from Huang et al. with sensor **S2** did not exhibit this  
242 interference from copper at pH 7, probably because copper was only five times in excess  
243 compared to mercury [15]. We can thus conclude that using realistic metal ions concentrations  
244 is clearly necessary to study selectivity and optimize analytical conditions of a new sensor for  
245 real life application, especially in the environmental field.

#### 246 3.2.4. Comparison with other rhodamine sensors

247 Sensors for mercury detection can be based on rhodamine, fluorescein, coumarin or dansyl  
248 organic dyes [5]. Among them, rhodamine sensors gives the best analytical performances, and  
249 we thus decided to compare our sensor **S1** with other rhodamine sensors described for  
250 applications in aqueous media (Table 3). From this comparison, we can conclude that sensor  
251 **S1** is the only sensor for which sensitivity and selectivity have been demonstrated for  
252 application to real natural water samples.

253

254

Ref	LOD ( $\mu\text{g}\cdot\text{L}^{-1}$ )	Selectivity
17	4.6	Demonstrated with 1 eq of interferent ions
20	14.8	Interference of $\text{Fe}^{3+}$ , others demonstrated with 5 eq of interferents ions
21	136	Demonstrated with 30 eq of interferent ions
12	470	Demonstrated with 1 eq of interferent ions
13	0.5	Interference of $\text{Zn}^{2+}$ , others demonstrated with 5 eq of interferents ions
16	0.3	Demonstrated with 1 eq of interferent ions
10	0.6	Demonstrated with 5 eq of interferent ions
This work	0.27	Demonstrated with concentration of interferent ions relevant with the analysis of natural water samples (up to 1000 eq for $\text{Cu}^{2+}$ and 200.000 eq for $\text{Ca}^{2+}$ )

255 Table 3. Comparative study of rhodamine-based sensor for  $\text{Hg}^{2+}$  analysis in aqueous media.

256

### 257 3.3. Test with real samples

258 Our optimized protocol was then applied to four real water samples (one tap water and three  
259 river samples) to assess the potential of our analytical procedure. Most publications related to  
260 mercury sensors describe application to quantify  $\text{Hg}^{2+}$  levels in living cells, with incubation  
261 levels at 20-40  $\mu\text{g}\cdot\text{L}^{-1}$  (100-200 nM) [10,11]. Application to environmental samples like natural  
262 waters requires lower levels of study. As our selected samples contained no mercury (checked  
263 by ICP-MS analysis), samples were spiked at 1  $\mu\text{g}\cdot\text{L}^{-1}$  (5 nM) and 2  $\mu\text{g}\cdot\text{L}^{-1}$  (10 nM) of mercury.  
264 As pH control is important for our protocol (use of an acetic acid buffer at pH 5.25), pH of the  
265 real samples was set between 5.2 and 5.3 after spiking. Results for the spiked samples show  
266 that good recoveries were achieved (Table 4), demonstrating that our protocol can be applied

267 to real water samples, even at the  $\mu\text{g.L}^{-1}$  level which is the parametric value for the quality of  
268 water intended for human consumption in Europe.

269

270

Sample	Spiked concentration of $\text{Hg}^{2+}$ ( $\mu\text{g.L}^{-1}$ )	Found ( $\mu\text{g.L}^{-1}$ )	Recovery (%)
Tap water	1	$0.95 \pm 0.11$	95.0
	2	$1.91 \pm 0.1$	95.5
River 1	1	$1.01 \pm 0.09$	101.0
	2	$1.88 \pm 0.06$	94.0
River 2	1	$0.88 \pm 0.07$	88.0
	2	$1.98 \pm 0.06$	99.0
River 3	1	$0.96 \pm 0.1$	96.0
	2	$1.87 \pm 0.08$	93.5

271 Table 4. Detection of  $\text{Hg}^{2+}$  in spiked real water samples using the microplate protocol. Buffer:  
272 Acetic acid 50 mM pH 5.25.

273

#### 274 4. Conclusions

275 In conclusion, this study has proven that simple optimizations of a metal ion detection method  
276 can result in large enhancement of the analytical performances, required for reliable application  
277 to real samples. Replacing rhodamine-B fluorophore by rhodamine-6G on our NS2-containing  
278 sensor improved detection limits more than 3-fold. Optimization of the buffer used for detection  
279 of  $\text{Hg}^{2+}$  ion displayed significant effects both on detection limits and selectivity. Acetate buffer

280 enabled detection of  $\text{Hg}^{2+}$  below  $1 \mu\text{g.L}^{-1}$  ( $\text{LOD} = 0.3 \mu\text{g.L}^{-1}$ ), whereas traditional neutral  
281 buffers were limited at  $2 \mu\text{g.L}^{-1}$ . Use of acetate buffer also circumvented the problem of copper  
282 in competitive experiments, which is a very common issue related to copper as a general  
283 fluorescent quencher [22]. The optimized procedure has been successfully applied to real water  
284 samples, demonstrating applicability of our new methodology for  $\text{Hg}^{2+}$  detection.

285

## 286 **Acknowledgements**

287 The project leading to this publication has received funding from the French Research Agency  
288 (project « SMART-3D », ANR-18-CE04-0005). Financial support from Aix-Marseille  
289 Université, the Centre National de la Recherche Scientifique (CNRS), and Centrale Marseille  
290 is also gratefully acknowledged.

291

## 292 **References**

293 [1] C. M. L. Carvalho, E.-H. Chew, S. I. Hashemy, J. Lu, A. Holmgren, Inhibition of the human  
294 thioredoxin system, a molecular mechanism of mercury toxicity, *J. Biol. Chem.* 283 (2008)  
295 11913-11923. <https://doi.org/10.1074/jbc.M710133200>.

296 [2] G.Bjørklund, M. Dadar, J. Mutter, J. Aaseth, The toxicology of mercury: Current research  
297 and emerging trends, *Environ. Res.* 159 (2017) 545-554.  
298 <https://doi.org/10.1016/j.envres.2017.08.051>

299 [3] A. Manceau, M. Enescu, A. Simionovici, M. Lanson, M. Gonzalez-Rey, M. Rovezzi, R.  
300 Tucoulou, P. Glatzel, K. L. Nagy, J.-P. Bourdineaud, Chemical forms of mercury in human hair  
301 reveal sources of exposure, *Environ. Sci. Technol.* 50 (2016) 10721-10729.  
302 <https://doi.org/10.1021/acs.est.6b03468>.

303 [4] T. Rasheed, M. Bilal, F. Nabeel, H. M.N. Iqbal, C. Li, Y. Zhou, Fluorescent sensor based  
304 models for the detection of environmentally-related toxic heavy metals, *Sci. Total Environ.* 615  
305 (2018) 476-485. <https://doi.org/10.1016/j.scitotenv.2017.09.126>.

- 306 [5] N. De Acha, C. Elosúa, J. M. Corres, F. J. Arregui, Fluorescent sensors for the detection of  
307 heavy metal ions in aqueous media, *Sensors* 19 (2019) 599. <https://doi.org/10.3390/s19030599>.
- 308 [6] H. M. Al-Saidi, A. A. El-Bindary, A. Z. El-Sonbati, M. A. Abdel-Fadeel, Fluorescence  
309 enhancement of rhodamine B as a tool for the determination of trace and ultra-trace  
310 concentrations of bismuth using dispersive liquid–liquid microextraction, *RSC Adv.* 6 (2016)  
311 21210-21218. <https://doi.org/10.1039/c5ra27764g>
- 312 [7] G. Chen, Z. Guo, G. Zeng, L. Tanga, Fluorescent and colorimetric sensors for environmental  
313 mercury detection, *Analyst* 140 (2015) 5400-5443. <https://doi.org/10.1039/c5an00389j>.
- 314 [8] M. H. Lee, J.-S. Wu, J. W. Lee, J. H. Jung, J. S. Kim, Highly sensitive and selective  
315 chemosensor for Hg<sup>2+</sup> based on the rhodamine fluorophore, *Org. Lett.* 9 (2007) 2501-2504.  
316 <https://doi.org/10.1021/ol0708931>.
- 317 [9] D. Wu, W. Huang, C. Duan, Z. Lin, Q. Meng, Highly sensitive fluorescent probe for  
318 selective detection of Hg<sup>2+</sup> in DMF aqueous media, *Inorg. Chem* 46 (2007) 1538-1540.  
319 <https://doi.org/10.1021/ic062274e>.
- 320 [10] Y.-J. Gong, X.-B. Zhang, Z. Chen, Y. Yuan, Z. Jin, L. Mei, J. Zhang, W. Tan, G.-L. Shen,  
321 R.-Q. Yu, An efficient rhodamine thiospirolactam-based fluorescent probe for detection of Hg<sup>2+</sup>  
322 in aqueous samples, *Analyst* 137 (2012) 932–938. <https://doi.org/10.1039/C2AN15935J>
- 323 [11] M. De la Cruz-Guzman, A. Aguilar-Aguilar, L. Hernandez-Adame, A. Bañuelos-Frias,  
324 F. J Medellín-Rodríguez, G. Palestino, A turn-on fluorescent solid-sensor for Hg(II) detection,  
325 *Nanoscale Res. Lett.* 9 (2014) 1-9. <https://doi.org/10.1186/1556-276X-9-431>.
- 326 [12] M. Li, Y. Sun, L. Dong, Q.-C. Feng, H. Xu, S.-Q. Zang, T. C.W. Mak, Colorimetric  
327 recognition of Cu<sup>2+</sup> and fluorescent detection of Hg<sup>2+</sup> in aqueous media by a dual chemosensor  
328 derived from rhodamine B dye with a NS2 receptor, *Sens. Actuat. B – Chem.* 226 (2016) 332-  
329 341. <https://doi.org/10.1016/j.snb.2015.11.132>.
- 330 [13] W. Huang, C. Song, C. He, G. Lv, X. Hu, X. Zhu, C. Duan, Recognition preference of  
331 rhodamine-thiospirolactams for Mercury(II) in aqueous solution, *Inorg. Chem.* 48 (2009) 5061-  
332 5072. <https://doi.org/10.1021/ic8015657>.
- 333 [14] W. Lin, X. Cao, Y. Ding, L. Yuan, Q. Yu, A reversible fluorescent Hg<sup>2+</sup> chemosensor  
334 based on a receptor composed of a thiol atom and an alkene moiety for living cell fluorescence



335 imaging, *Org. Biomol. Chem.* 8 (2010) 3618-3620. <https://doi.org/10.1039/C0OB00081G>.

336 [15] J. Huang, Y. Xu, X. Qian, A Rhodamine-based Hg<sup>2+</sup> sensor with high selectivity and  
337 sensitivity in aqueous solution: a NS2-containing receptor, *J. Org. Chem.* 74 (2009) 2167-2170.  
338 <https://doi.org/10.1021/jo802297x>.

339 [16] J. Gong, C. Liu, X. Jiao, S. He, L. Zhao and X. Zeng, A novel near-infrared fluorescent  
340 probe with improved Stokes shift for specific detection of Hg<sup>2+</sup> in mitochondria, *Org. Biomol.*  
341 *Chem.* 18 (2020) 5238-5244. <https://doi.org/10.1039/D0OB00507J>

342 [17] F. Pan, J. Mao, Q. Chen, P. Wang, Solid-phase extraction of mercury(II) with magnetic  
343 core-shell nanoparticles, followed by its determination with a rhodamine-based fluorescent  
344 probe, *Microchim. Acta* 180 (2013) 1471-1477. <https://doi.org/10.1007/s00604-013-1084-6>

345 [18] J. L. Parker, N. S. Bloom, Preservation and storage techniques for low-level aqueous  
346 mercury speciation, *Sci. Total Environ.* 337 (2005) 253-263.  
347 <https://doi.org/10.1016/j.scitotenv.2004.07.006>

348 [19] ANNEXES to the Proposal for a Directive of the European Parliament and of the Council  
349 on the quality of water intended for human consumption (recast), European Commission,  
350 COM(2017) 753 final 2017/0332.  
351 [https://eur-lex.europa.eu/resource.html?uri=cellar:8c5065b2-074f-11e8-b8f5-](https://eur-lex.europa.eu/resource.html?uri=cellar:8c5065b2-074f-11e8-b8f5-01aa75ed71a1.0016.02/DOC_2&format=PDF)  
352 [01aa75ed71a1.0016.02/DOC\\_2&format=PDF](https://eur-lex.europa.eu/resource.html?uri=cellar:8c5065b2-074f-11e8-b8f5-01aa75ed71a1.0016.02/DOC_2&format=PDF)

353 [20] F. Yan, D. Cao, M. Wang, N. Yang, Q. Yu, L. Dai, L. Chen, A New Rhodamine-Based  
354 “Off-On” Fluorescent Chemosensor for Hg (II) Ion and its Application in Imaging Hg (II) in  
355 Living Cells, *J. Fluoresc.* 22 (2012) 1249-1256. <https://doi.org/10.1007/s10895-012-1065-x>

356 [21] X. Li, R. Zhao, Y. Wei, D. Yang, Z. Zhou, J. Zhang, Y. Zhou, A rhodamine derivative for  
357 Hg<sup>2+</sup>-selective colorimetric and fluorescent sensing and its application to in vivo imaging, *Chin.*  
358 *Chem. Lett.* 27 (2016) 813-816. <https://doi.org/10.1016/j.ccllet.2016.04.001>

359 [22] S. Mizukami, T. Nagano, Y. Urano, A. Odani, K. Kikuchi, A fluorescent anion sensor that  
360 works in neutral aqueous solution for bioanalytical application, *J. Am. Chem. Soc.* 124 (2002)  
361 3920-3925. <https://doi.org/10.1021/ja0175643>.

362

363

364

365 **Figure captions**

366 *Figure 1. Structure of sensors S1 and S2.*

367 *Figure 2- Fluorescence emission spectra of sensors S1 and S2 in the presence of different*  
368 *concentrations of Hg<sup>2+</sup>. Excitation was performed at 535 nm. Protocol: 1 mL sample + 150  $\mu$ L*  
369 *HEPES buffer 50 mM pH 7.0 + 100  $\mu$ L sensor 5  $\mu$ M, shaking for 3 min. Inset: Zoom for*  
370 *fluorescence intensity between 0 and 10.*

371 *Figure 3- Comparison of the response of S1 with two standard solutions, depending on the*  
372 *buffer. Microplate protocol. Buffer: Acetic acid 50 mM for pH 5-5.5; MES 50 mM for pH 6-*  
373 *6.5; MOPS 50 mM for pH 7-8. (A) Fluorescence intensities; (B) Ratio of fluorescence intensities*  
374 *between standard solutions and blank ( $F_2/F_0$ : ratio Hg 2  $\mu$ g.L<sup>-1</sup>/blank;  $F_{10}/F_0$ : ratio Hg 10*  
375  *$\mu$ g.L<sup>-1</sup>/blank).*

376 *Figure 4- Influence of the sensor S1 concentration on the fluorescence response. Microplate*  
377 *protocol. Sensor concentration is the concentration in the 25  $\mu$ L of sensor added to the sample.*  
378 *Buffer: Acetic acid 50 mM pH 5.25.  $F_5/F_0$  is the ratio between the fluorescence response of a 5*  
379  *$\mu$ g.L<sup>-1</sup> standard solution and the blank.*

380 *Figure 5. Selectivity study with sensor S1. A. Buffer: Acetic acid 50 mM pH 5.25. B: Buffer:*  
381 *MOPS 50 mM pH 7.1. Microplate protocol,  $F/F_0$  is the ratio between the fluorescence response*  
382 *of the metal ions solution and the blank.*

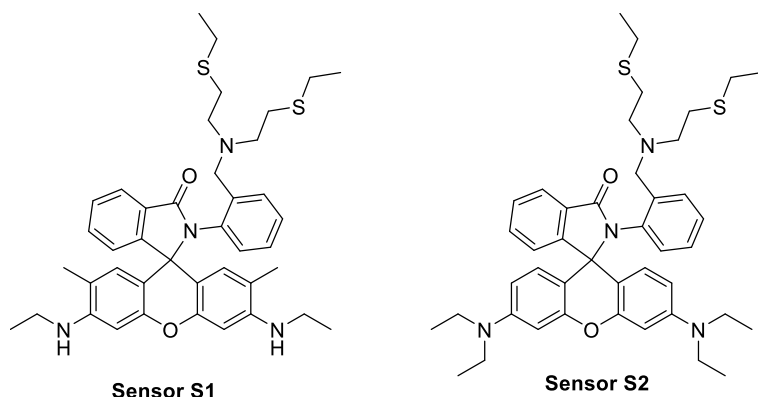
383 *Scheme 1. Synthesis of Sensor S1*

384

385

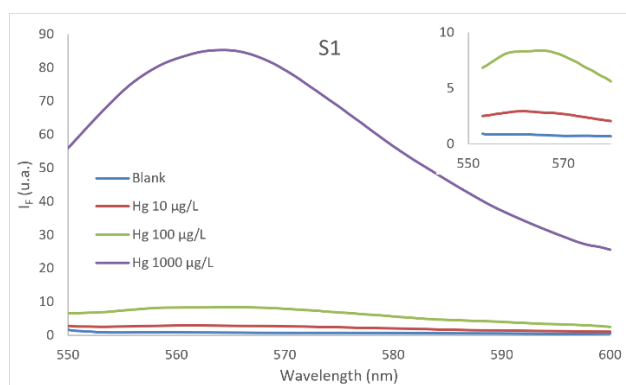
386

387

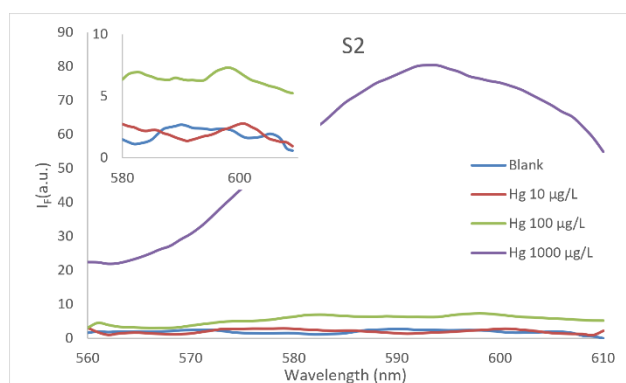


389 **Figure 1.** Structure of sensors **S1** and **S2**

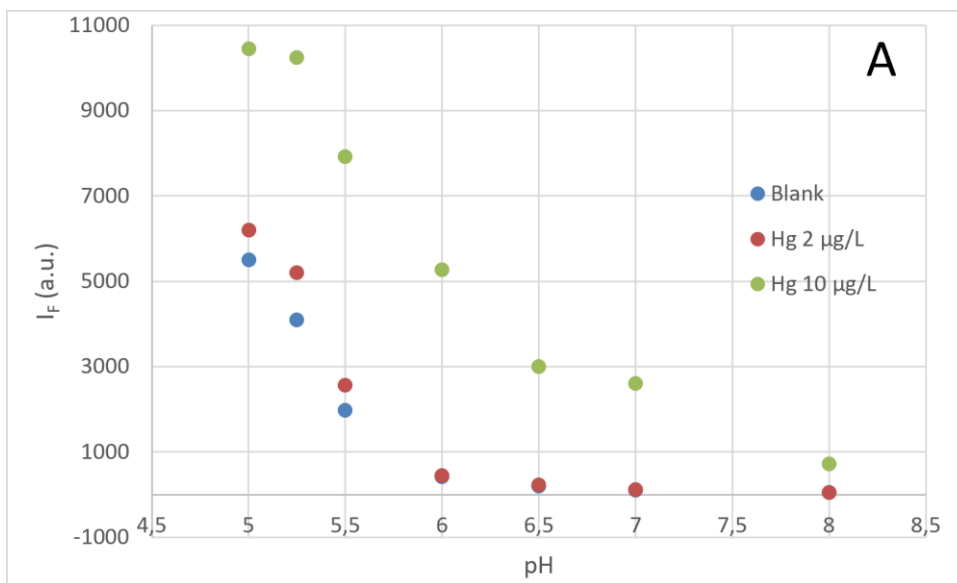
390



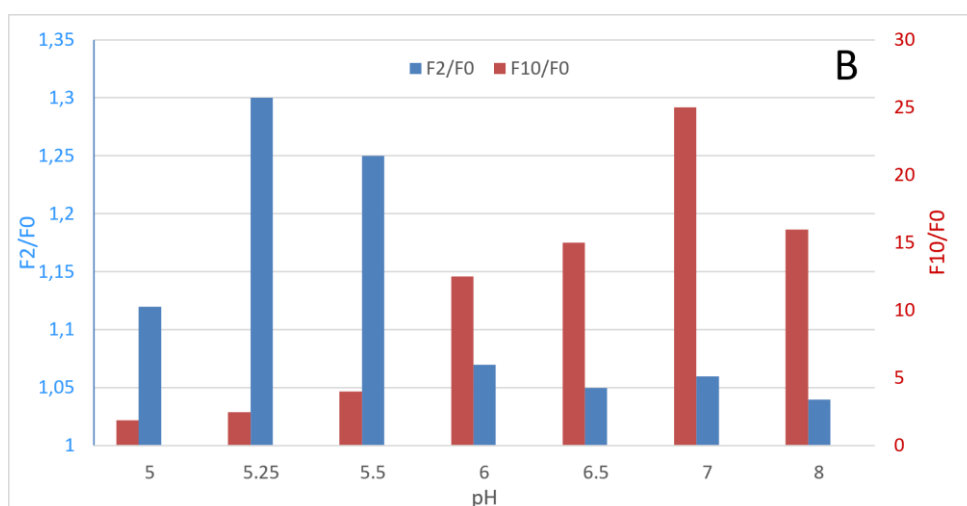
392



393 **Figure 2.** Fluorescence emission spectra of sensors **S1** and **S2** in the presence of different  
 394 concentrations of  $\text{Hg}^{2+}$ . Excitation was performed at 535 nm. Protocol: 1 mL sample + 150  $\mu\text{L}$   
 395 HEPES buffer 50 mM pH 7.0 + 100  $\mu\text{L}$  sensor 5  $\mu\text{M}$ , shaking for 3 min. Inset: Zoom for  
 396 fluorescence intensity between 0 and 10

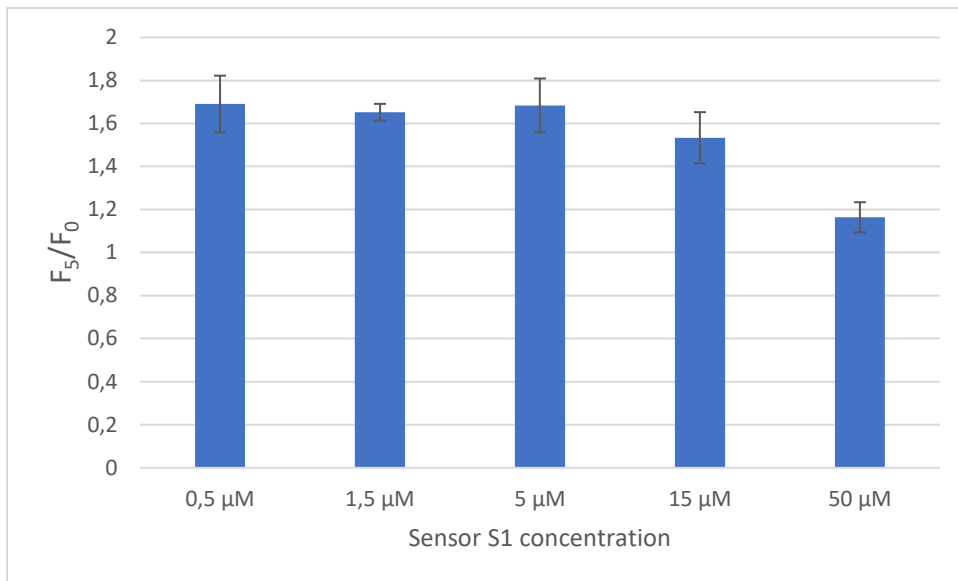


397



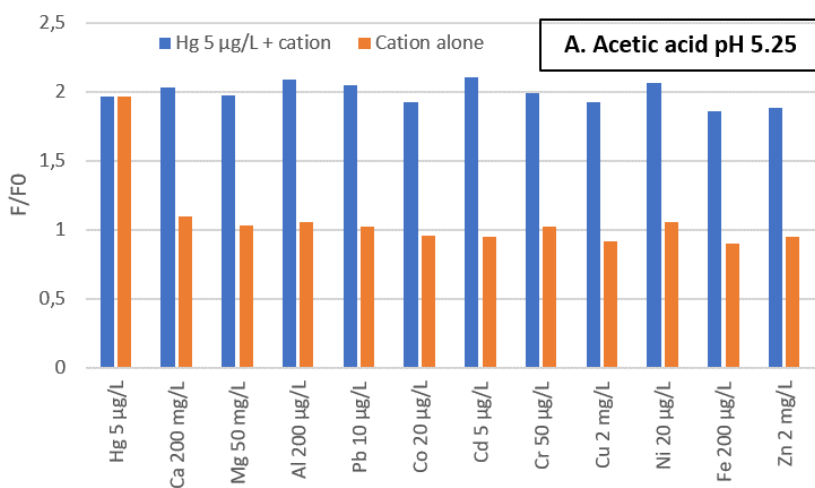
398

399 **Figure 3.** Comparison of the response of **S1** with two standard solutions, depending on the  
 400 buffer. Microplate protocol. Buffer: Acetic acid 50 mM for pH 5-5.5; MES 50 mM for pH 6-  
 401 6.5; MOPS 50 mM for pH 7-8. (A) Fluorescence intensities; (B) Ratio of fluorescence  
 402 intensities between standard solutions and blank (F2/F0: ratio Hg 2 µg.L<sup>-1</sup>/blank; F10/F0: ratio  
 403 Hg 10 µg.L<sup>-1</sup>/blank)

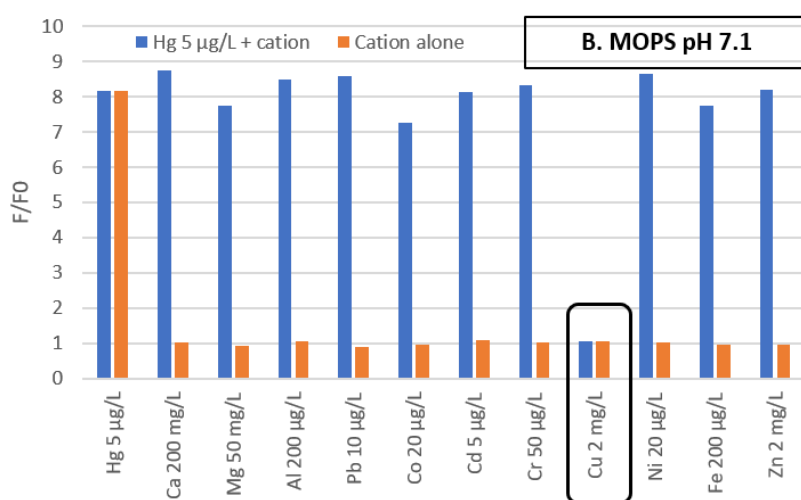


404

405 **Figure 4.** Influence of the sensor **S1** concentration on the fluorescence response. Microplate  
406 protocol. Sensor concentration is the concentration in the 25 μL of sensor added to the sample.  
407 Buffer: Acetic acid 50 mM pH 5.25.  $F_5/F_0$  is the ratio between the fluorescence response of a 5  
408 μg.L<sup>-1</sup> standard solution and the blank

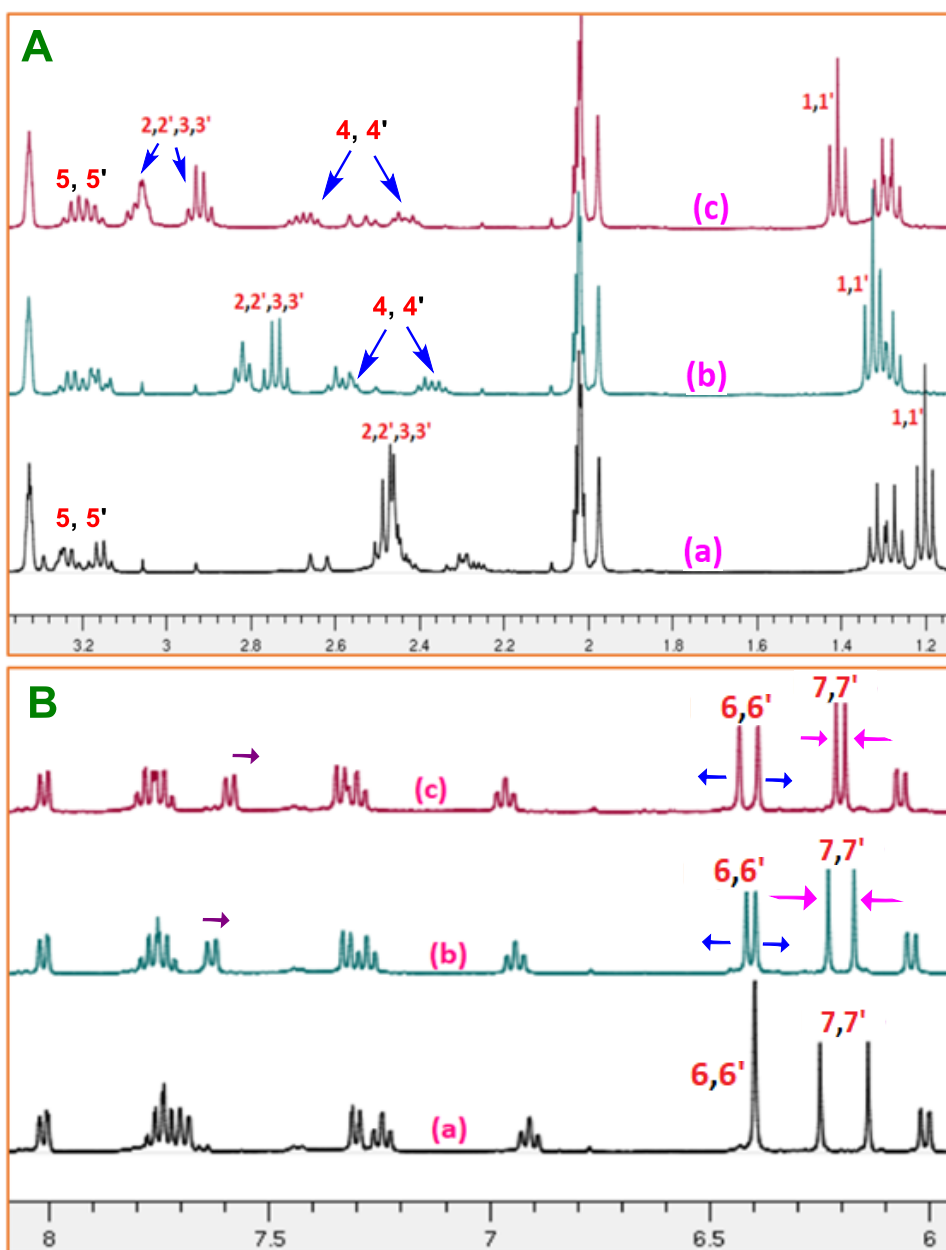


409



410

411 **Figure 5.** Selectivity study with sensor **S1**. A. Buffer: Acetic acid 50 mM pH 5.25. B: Buffer:  
 412 MOPS 50 mM pH 7.1. Microplate protocol, F/F0 is the ratio between the fluorescence response  
 413 of the metal ions solution and the blank



414

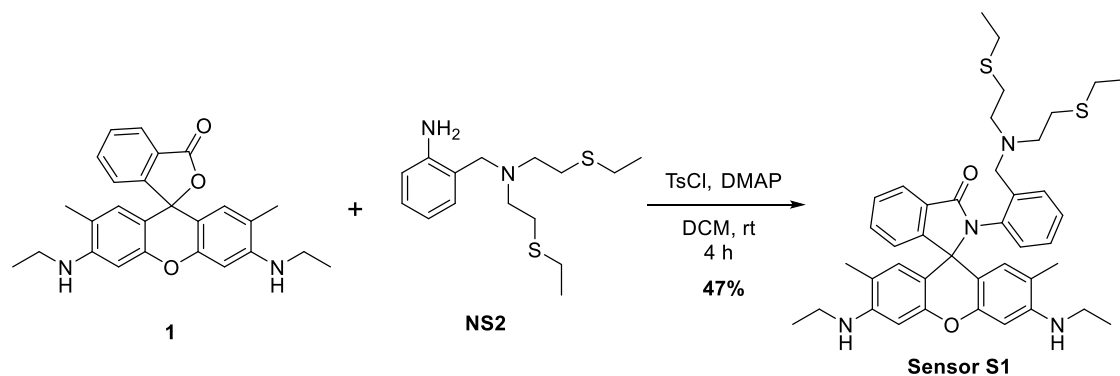
415 Figure 6.  $^1\text{H-NMR}$  titration of Sensor **S1** (10.0 mM) with  $\text{Hg}^{2+}$  in  $\text{CD}_3\text{CN}$  and  $\text{CD}_3\text{OD}$  (1:1).

416 (a) Sensor **S1** only; (b) Sensor **S1** + 0.5 equiv of  $\text{Hg}^{2+}$  and (c) Sensor **S1** + 1.00 equiv of  $\text{Hg}^{2+}$

417

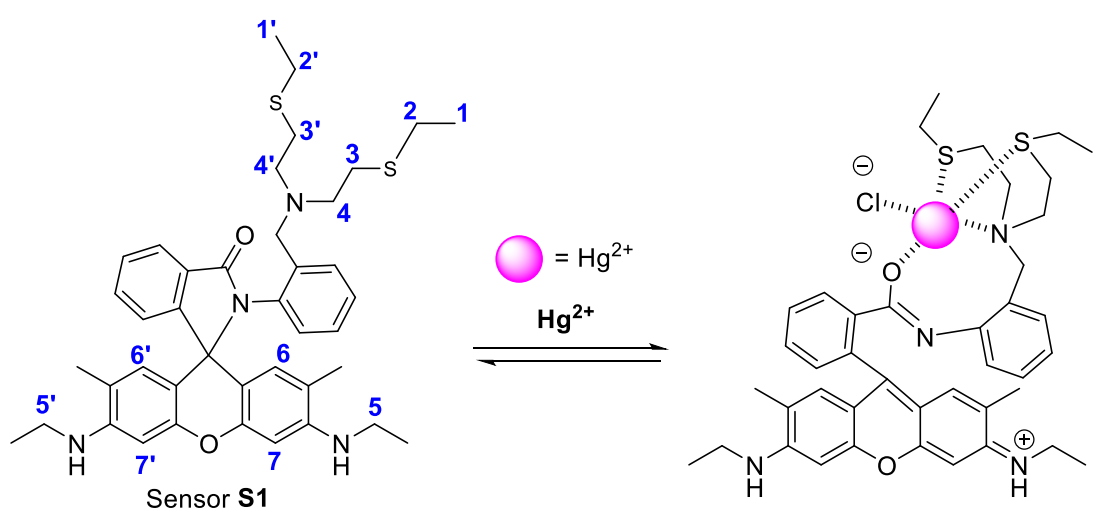
418

419



420

421 **Scheme 1.** Synthesis of Sensor S1



422

HRMS (ES<sup>+</sup>):  $[\text{M}+\text{H}]^+ = 695.3761$

HRMS (ES<sup>+</sup>):  $[\text{M}+\text{Hg}+\text{Cl}]^+ = 931.3174$

423 **Scheme 2.** Proposed mode of complexation of Sensor S1 with  $\text{Hg}^{2+}$

424

425

426

427

428